Available online at www.sciencedirect.com
SCIENCE DIRECT®
Chemical Physics 318 (2005) 82–90
Chemical Physics
www.elsevier.com/locate/chemphys

Wavefunction engineering: From quantum wells to near-infrared type-II colloidal quantum dots synthesized by layer-by-layer colloidal epitaxy

J. Jack Li [a], James M. Tsay [a], Xavier Michalet [a], Shimon Weiss [a,b,c,*]

[a] Department of Chemistry and Biochemistry, University of California at Los Angeles, 607 Charles E Young Drive East, Los Angeles, CA 90095, USA
[b] Department of Physiology, University of California at Los Angeles, Los Angeles, CA 90095, USA
[c] California NanoSystems Institute, University of California at Los Angeles, Los Angeles, CA 90095, USA

Received 21 December 2004; accepted 19 April 2005
Available online 6 June 2005

Abstract

We review the concept and the evolution of bandgap and wavefunction engineering, the seminal contributions of Dr. Chemla to the understanding of the rich phenomena displayed in epitaxially grown quantum confined systems, and demonstrate the application of these concepts to the colloidal synthesis of high quality type-II CdTe/CdSe quantum dots using successive ion layer adsorption and reaction chemistry. Transmission electron microscopy reveals that CdTe/CdSe can be synthesized layer by layer, yielding particles of narrow size distribution. Photoluminescence emission and excitation spectra reveal discrete type-II transitions, which correspond to energy lower than the type-I bandgap. The increase in the spatial separation between photoexcited electrons and holes as a function of successive addition of CdSe monolayers was monitored by photoluminescence lifetime measurements. Systematic increase in lifetimes demonstrates the high level of wavefunction engineering and control in these systems.

1. Introduction

The information technology revolution is attributed to the invention of the transistor. The power of the transistor was fully utilized, however, only after the introduction of the integrated circuit (IC). The need to use semiconductors not only for transistors and diodes, but also for resistors and capacitors in order to implement a full circuit on the same substrate, required the development of a key technology – the precise deposition of thin layers of different semiconducting compositions. Initially, layers containing different dopants were fabricated to better control charge carriers (electrons and holes) in their respective (conduction and valence) bands. Soon after, different semiconductors compositions were combined into single-, double- and multi-heterostructures, and the field of 'bandgap engineering' has emerged [1].

In particular, the double-heterostructures (DHs) composed of a low-bandgap material sandwiched between two wide-bandgap layers afforded efficient electron and hole injection into the middle layer, leading to efficient room temperature CW lasing in semiconducting materials. The DH laser was a precursor for what has become to be known as the "quantum-well" structure. The advances in atomically precise deposition methods such as molecular beam epitaxy (MBE) [2,3] and metalorganic chemical vapor deposition (MOCVD)

* Corresponding author.
E-mail addresses: jtsay@chem.ucla.edu (J.M. Tsay), sweiss@chem.ucla.edu (S. Weiss).

0301-0104/$ - see front matter © 2005 Elsevier B.V. All rights reserved.
doi:10.1016/j.chemphys.2005.04.029

[4] allowed the deposition of a precise ultrathin middle layer of a lower bandgap, where charge carriers experienced quantum confinement effects. This development has expanded 'bandgap engineering' into 'wavefunction engineering', giving the control of the band gap energy, refractive index, carrier mass and mobility, excited state lifetime and many other fundamental parameters. A slew of devices and applications ensued, including low-threshold semiconductor lasers, high-efficiency light-emitting diodes, solar cells and photodetectors, semiconductor integrated optics components, heterojunction bipolar transistors (HBTs), two-dimensional electron-gas field-effect transistors (TEGFET), resonance-tunneling diodes, efficient photocathodes and infrared quantum cascade lasers [1].

Beyond these remarkable technological feats, the ability to synthesize almost-perfect artificial quantum structures afforded the engineering of confined electronic eigenfunctions in a manner never possible before. The quantum well structure formed a perfect 'laboratory' for the exploration of fundamental quantum mechanical phenomena, such as the transport properties of two-dimensional electron gas; quantum Hall effect; fractional quantum Hall effect; resonance tunneling; coherent excitations in superlattices, and of particular interest for this special issue and this work, the observation and study of excitons at room temperature.

Bulk excitons in large bandgap semiconductor materials exhibit large optical and electro-optical nonlinearities at low temperatures [5]. However, when excitons are confined into ultra-thin semiconductor layers, large changes to the linear absorption and strong optical nonlinearities are resulted even at room temperature [6,7]. When coupled with external fields, large Stark shifts could be observed [8] and utilized [9]. When subjected to femtosecond pulses, nonthermal relaxation of excitons in quantum wells could be observed [10]. Following these ground-breaking studies, many ultrafast and many-body nonlinear effects were carefully investigated [11,12]. More recently, macroscopic coherences and quantum liquid behaviors were observed for these confined excitonic systems [13–16].

In the band alignment of the quantum well systems described above, both electrons and holes (and therefore excitons) are confined to the smaller bandgap, middle layer (referred to as type-I quantum wells). In staggered, type-II systems, either the valence or the conduction band of the narrower-gap material lies outside the bandgap of the other material, forming an indirect gap in real space. Photoexcitation of carriers in opposite layers of the structure results in charge separation, reduced oscillator strength and reduced emission. Subsequent recombination occurs across the interface on a slower time scale (longer radiative lifetime). The emission energy is reduced (red-shifted) by the band offset at the interface and is below the bandgap of either of the layers [17].

The ability to construct heterostructures of even lower dimensions gave forth the study and exploration of quantum confinement in one dimension (quantum wire) and even zero dimension (quantum dot). This opened up the possibilities to study the behavior of one- and zero-dimensional electron gas, produce one- and zero-dimensional density of states with sharp maxima, increased exciton binding energy, introduce stronger excitonic nonlinearities [18,19], construct "single-electron" transport devices and further improve semiconductor lasers by reducing lasing threshold, increasing differential gain and diminishing temperature dependence of the gain [1].

Important recent advances include the development of colloidal semiconductor quantum dots [20] and the proposal for their use in biology and medicine [21,22]. The exponential growth of this field is reviewed [23]. To-date, most colloidal qdots have been synthesized from materials compositions that result in band alignment of type-I. Examples of these systems are CdSe, CdTe, InAs, and InP. As in two-dimensional quantum wells, the larger bandgap overcoating (shell) increases the quantum yield and photostability of the core.

Qdots emitting in the far-red and near-infrared (NIR) regions of the spectrum are of great interest for in vivo biological imaging, diagnostics, and possibly even therapeutics, due to separation from autofluorescence background and increased penetration of excitation and emission light through thick tissues. One possible way to achieve NIR qdots is through the red-shift introduced by staggered band alignment (see above). Recently, Kim et al. [24] succeeded in synthesizing CdTe/CdSe type-II NIR colloidal qdots and demonstrated their use in background-free imaging of a pig's lymph node during a surgical procedure [25].

Similarly to staggered quantum wells, photoexcitation of type-II qdots results in charge separation of one type charge carrier in the core and the opposite sign charge carrier in the shell (Fig. 1). Radiative

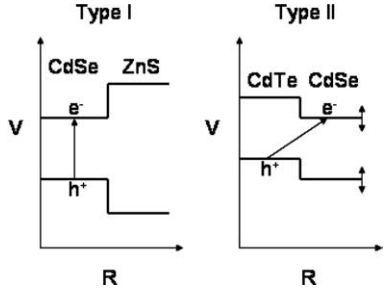

Fig. 1. (Left) A cartoon of band offsets of type-I CdSe/ZnS QDs as a function of distance from the center. Electrons and holes stay in CdSe after photoexcitation. (Right) A cartoon of band offsets of type-II CdTe/CdSe QDs as a function of distance from the center. Electrons are confined to CdSe and holes confined to CdTe after photoexcitation.

recombination in this arrangement is very sensitive to defects at the core–shell interface. An accurate atomic layer colloidal deposition, in analogy to MBE, is therefore highly desirable for the synthesis of high quality NIR type-II qdots.

It has been recently shown that layer-by-layer epitaxial growth could be achieved in solution by successive ion layer adsorption and reaction (SILAR) [26]. This method has been used with half monolayer accuracy to synthesize type-I core/shells and quantum well qdots [27] with small size distribution and high quantum yield.

Here, we demonstrate the synthesis of high quality NIR type-II qdots using SILAR. We characterize the photophysical properties of these QDs with each monolayer of shell grown using absorption, photoluminescence excitation, fluorescence emission and fluorescence lifetime spectroscopies. Their structural properties are characterized by transmission electron microscopy (TEM). The precise control of these sophisticated zero-dimensional, staggered band alignment, type-II NIR quantum structures is a supreme manifestation of bandgap and wavefunction engineering, inspired by- and dedicated to- the work of one of its inventors, Dr. Daniel Simon Chemla.

2. Materials and methods

2.1. Chemicals

The following chemicals were obtained from Aldrich: cadmium oxide (99.99%), selenium (99.999%, 100 mesh), tellurium (99.8%, 200 mesh), oleic acid (tech. 90%), Octadecene (tech. 90%), octadecylamine (97%), and sulfur (flake, 99.99%). Tributylphosphine (99%, TBP) was made by Strem Chemicals. Zinc oxide (ACS certified, 100.3%) was purchased from Fisher. *n*-Tetradecylphosphonic acid (98%, TDPA) was from Alfa Aesar. All organic solvents were from EMD.

2.2. TEM measurements

Transmission electron microscopy images were collected at a magnification of 67,000 on a FEI Tecnai G12 equipped with an UltraScan 1000 CCD camera which is controlled by Gatan Microscopy Suite Software.

2.3. Optical measurements

All QD samples were dispersed in hexanes for optical measurements. Absorption spectroscopy was performed with a Perkin–Elmer Lambda 25 UV/vis Spectrometer. Photoluminescence emission and excitation spectra were acquired using a fluorimeter (Photon Technologies International) equipped with a 75 W Xe lamp and a Hammamatsu R928 photomultiplier tube (PMT). Software was used to correct for the quantum efficiency of the PMT up to 900 nm.

Photoluminescence excitation (PLE) was measured by probing the intensity dependence of the photoluminescence peak of the QDs with excitation wavelength. QDs were excited in a 200–300 nm range at smaller wavelengths than their PL peaks using a Xe lamp equipped with a monochromator. The emission was collected at a constant wavelength (within 1 nm accuracy) using a monochromator before the PMT at the QD's PL emission peak.

Lifetime measurements were taken using a custom-made time correlated single photon counting (TCSPC) apparatus. A femtosecond Ti:Sa laser (Mira 900, Coherent, Santa Clara, CA) pumped by a multiline Argon ion laser (Sabre, Coherent) was tuned to emit at 880 nm (repetition rate: 75.5 MHz). The repetition rate was decreased to a 2.375 MHz using an acousto-optical pulse-picker (Model 9200, Coherent). Four percent of the resulting intensity was sent to a fast PIN photodiode (DET210, Thorlabs, Newton, NJ), whose signal was fed to a fast pre-amplifier and discriminator (Model 9327, Ortec, Oak Ridge, TN) and used as a stop signal for the time-to-amplitude converter (TAC, Model 567, Ortec). The laser pulses were frequency doubled using a BBO crystal (Casix/Photop Technologies, Chatsworth, CA), collimated and expanded to overfill the back focal plane of a 60× 1.45 NA oil immersion objective (Olympus America, Melville, NY). The laser spot focused ~20 μm into the sample solution creating a fL excitation volume from which the emitted fluorescence was collected using the same objective lens. Excitation and emission were separated by a 500LP dichroic mirror (Chroma Technology, Rockingham, VT). A 100 μm pinhole placed at the focus of the tube lens of the inverted microscope (IX71, Olympus) rejected out-of-focus light. The emitted light was focused on a photon counting avalanche photodiode (APD, SPCM-AQR 14, Perkin–Elmer Optoelectronics, Fremont, CA) using achromatic relay lenses. Each detected photon results in the emission of a 30 ns TTL pulse, used as the start signal of the TAC after inversion (IT100, Ortec). A TAC window of 500 ns was used in all experiments. Synchronized readout of the TAC output by a fast 12bit ADC board (PXI-6115E, National Instruments, Austin, TX) and histograming of the timed-delay values (decay curves) was performed by a custom LabView software. The instrument response function (IRF) was acquired with a solution of erythrosin B. The fluorescence emission was filtered using a 650 nm long pass and 820 short pass filter. Deconvolution and multi-exponential fitting of the decay curves was performed using custom LabView software.

3. Results and discussion

3.1. SILAR chemistry for type-II QDs

The development of SILAR chemistry for type-II QDs was motivated by two factors: the desire to use stable precursors as alternatives to highly toxic and pyrophoric organometallic compounds such as dimethyl cadmium, and the need for well-controlled and precise deposition of shells which results in narrow size distribution and photoluminescence emission width. In accordance to recently developed "greener" approaches, CdO was used as the Cd source, replacing dimethyl cadmium in both the synthesis of CdTe cores and CdSe shells. CdTe core nanocrystals were made by injecting Te-TBP (tributylphosphine) into a hot solution composed of Cd-TDPA (tetradecylphosphonic acid) and 1-octadecene (ODE) [28]. These cores were purified to remove unreacted tellurium before shell overcoating.

In order to have precise deposition of shells, type-II CdTe/CdSe core/shell colloidal quantum dots were synthesized with a layer-by-layer colloidal epitaxy method [26]. Briefly, purified CdTe cores were mixed with two components: the coordinating ligands (oleic acid, octadecylamine or trioctylphosphine oxide), as a single component or their combination and a noncoordinating solvent (ODE) which was used as a substitute for TOPO. The reaction flask containing CdTe cores, ligands, and solvent was pumped down under vacuum at room temperature for 30 min. Then, the temperature was increased to 50 °C, and nitrogen was flowed into the reaction flask and used for the rest of the reaction. At a designated temperature, ca. 200 °C, one precursor solution, with the Cd (Se) source, was injected into the flask in a calculated amount corresponding to an overcoating of all the CdTe cores at once. The epitaxial growth of the single component rendered a red shift of both the absorption and the photoluminescence. Both absorption and emission spectra of aliquots were recorded to monitor the reaction and determine the next injection point. After a redshifted emission was no longer observed in an interval of 5 min, the injection of a second precursor solution, this time with the Se (Cd) source, was carried out. The full reaction of two successive injections (one for each cation/anion precursor) adds one monolayer of shell on top of the cores. Alternating injections were repeated until the desired number of CdSe layers was obtained. Because the injection amount is stoichiometric, no free precursor is left over. Due to the lack of coexistence of both precursors, there is no homogeneous nucleation even at high temperatures. Layer-by-layer colloidal epitaxy of heterostructured colloidal quantum dots with extremely high quality could be produced by SILAR, in a way very analogous to MBE. This method is especially useful for the synthesis of more complex heterostructures, such as CdTe/CdSe/CdS. The CdS type-I shell effectively increases the QY and photostability of type-II structures. More details about the synthesis will be reported elsewhere.

3.2. TEM

Transmission electron microscopy (TEM) was used to evaluate the size and shape of the CdTe/CdSe core/shell samples. After evaluating the TEM results, we found that the average diameters of the QDs with varying CdSe layers are consistent with the calculations for the amount of precursors injected (Fig. 2). Each injection of precursors corresponding to one monolayer of shell increases the diameter of the particles by 0.7 nm, in agreement with the lattice spacing of CdSe. In a previous study using the SILAR technique, it was found that TEM results of shell thickness agreed with the X-ray photoelectron spectroscopy (XPS) depth profile, which strongly suggested that the growth of the shell is indeed epitaxial [26].

The formation of a closely packed lattice of CdTe/CdSe QDs (of 3 shell layers) as measured by TEM (Fig. 2, right panel) is a good indication for narrow size distribution of the QDs. The controlled self-assembly of this lattice also provides evidence for the lack of CdSe core nucleation; i.e., CdSe is uniformly deposited only on the CdTe cores. Nearly spherical shapes of CdTe/CdSe were obtained after shell deposition via SILAR, in contrast to the growth of CdTe/CdSe tetrapods by a nonSILAR method [29]. It is likely that the controlled amount of precursors injected, calculated to be sufficient for only half a monolayer deposition at a time, prevents the formation of anisotropic shapes.

3.3. Absorption and emission spectroscopies

To study the effects of shell growth on fixed size cores, CdTe cores of 5.9 nm diameter were coated with 1, 2, or 3 monolayers of CdSe shell. As shown in Fig. 3, there are clear differences in the absorption spectra of CdTe with additional monolayers of CdSe. The absorption peaks continually redshift and lose their definition after each additional injection of shell precursors. After the addition of 3 shell monolayers, the excitonic features are completely lost. The spatially indirect nature of type-II transitions is responsible for the weaker absorption at the band edges. The transitions between the quantum levels of the valence band of CdTe and the conduction band of CdSe cannot be effectively detected in absorption, in contrast to type-I CdTe and CdSe QDs.

The photoluminescence emission spectra of CdTe/CdSe were also taken with the same series of different shell thickness samples from a single reaction (Fig. 4). As more layers of CdSe are deposited on CdTe cores, the emission of the QD redshifts, originating from the spatially indirect bandedge transition. This redshifted

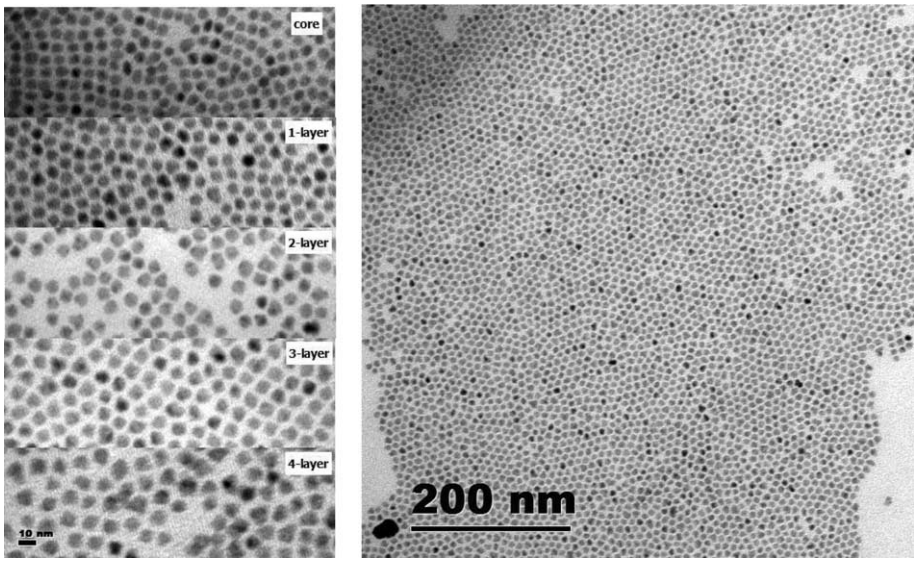

Fig. 2. TEM images of CdTe/CdSe type-II core/shell samples with successive layers of CdSe grown on a 5.9 nm CdTe core. These samples were synthesized by layer-by-layer colloidal epitaxy in a single reaction. The right figure corresponds to a superlattice of CdTe/CdSe with 3 monolayers of CdSe.

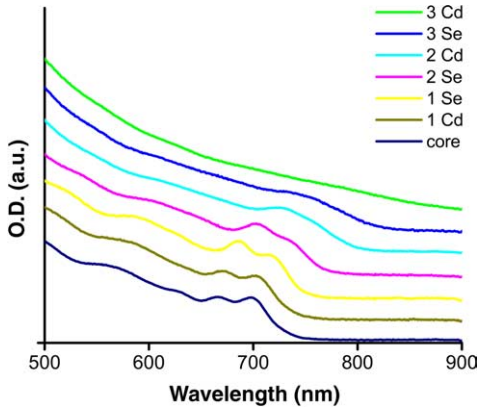

Fig. 3. Absorption spectra of CdTe QDs with varying CdSe shell thickness.

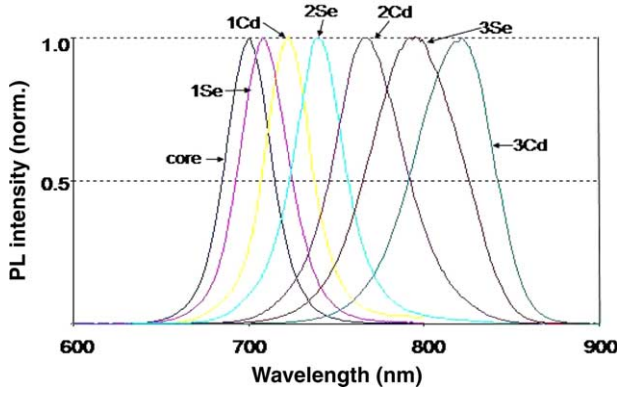

Fig. 4. Photoluminescence emission spectra of CdTe with varying CdSe shell thickness.

emission gives a direct measure of the energy difference between the valence band edge of CdTe and the conduction band edge of CdSe. The high QY and narrow emissions indicate that the NIR emission from SILAR prepared CdTe/CdSe is not from trap state photoluminescence. Large redshifts of both the absorption profile and photoluminescence emission with additional layers of CdSe provide evidence that type-II QDs have been indeed synthesized.

3.4. Comparison of absorption and photoluminescence excitation spectroscopy

Both absorption and photoluminescence excitation (PLE) spectra may be used to reveal the excitation wavelength dependence on the photoluminescence. Absorption spectroscopy, however, is limited by the fact that it measures the whole ensemble of absorption of QDs, meaning larger size distributions broaden the excitonic absorption peaks. In contrast, PLE spectra measure the dependence of PL intensity of QDs at a fixed wavelength on different excitation wavelengths. This enables the measurement of the absorption spectrum of a subpopulation in the sample to be taken, reducing size distribution broadening effects. Though differences in absorption spectra and PLE are much more pronounced for QDs at lower temperatures, PLE is especially important, even at room temperature, for samples with inhomogeneities in emission. These inhomogeneities are dependent on the success of SILAR reactions for type-II QDs. In particular, we have noticed that unsuccessful SILAR reactions and oxidized type-II QDs resulted in

two populations of emissions (type-I and type-II emissions in the same sample). PLE was used to effectively narrow the excitation dependence on the peak type-II emission.

It was previously shown that the excitonic peaks in the absorption spectra of CdTe/CdSe quantum dots vanish after sufficient CdSe shell was deposited on the CdTe core [24]. In this study, we also found that SILAR synthesized CdTe/CdSe QDs with $\geqslant 3$ CdSe monolayers yielded featureless absorption spectra. There are several possibilities for this observation: (i) very large size distributions of core/shell particles are obtained; (ii) the sharp type-I transitions all vanish from the conversion to the more weakly absorbing type-II transitions; (iii) there is an inhomogeneous broadening due to many more states available from the added complexity of the structure; (iv) strong scattering due to aggregation masks weak excitonic features [30].

Due to the relatively narrow size distribution of these particles as measured by TEM, it is surprising that the PLE spectra reveal features not found in the absorption spectra (Fig. 5). For CdTe QDs, the PLE spectra and absorption spectra are in good agreement, and all expected excitonic transitions are found in both, as for CdSe QDs. In type-II QDs, however, excitonic features

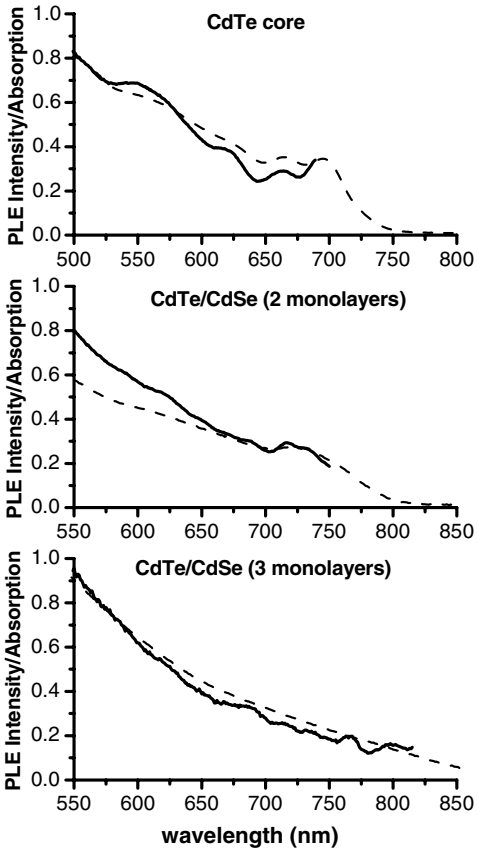

Fig. 5. Photoluminescence excitation (solid line) and absorption data (dashed line) of CdTe cores, CdTe/CdSe (2 monolayers CdSe) and CdTe/CdSe (3 monolayers CdSe).

associated with electronic transitions from the core to the shell are clearly observed by PLE, while not present in the absorption spectra (Fig. 5). With additional layers of shells, the main excitonic peak from the type-I transition ($1S_e$–$1S_{3/2}$) begins to vanish, while new peaks arise with less energy than the original band gap of CdTe. These features show that type-II quantum dots have discrete transitions from the valence states of CdTe to the conduction states of CdSe which arise from quantum confinement. With 2 monolayers of CdSe shell, multiple peaks are revealed in the PLE in contrast to one broad peak found in the absorption spectra. Finally, while all excitonic features are washed out in the absorption of particles with 3 shell monolayers, the PLE shows as many as five features. Again, these peaks correspond to transitions of lower energy compared to the original CdTe bandgap. These results were reproducible for different batches of SILAR reactions of CdTe/CdSe QDs.

The PLE-observed absorption peaks are of considerably smaller amplitude than type-I PLE peaks. This could be explained by the weaker oscillator strength due to spatial separation of the carriers in type-II structures. After the deposition of several CdSe layers, it is apparent from both the PLE spectrum and emission spectrum that there is no residual type-I excitonic transition of appreciable strength left. Strong type-I transitions in type-II heterostructures may only be present when the conduction bands of the two materials have different symmetry, since there needs to be a potential barrier at the interface to keep the carriers from separating into the different layers. Because the conduction bands of CdTe and CdSe are both Γ states (have minima at $k = 0$), the type-I transition of CdTe should be completely suppressed with addition of CdSe layers.

It is important to mention that even PLE spectra can fail to resolve excitonic peaks from type-II structures because different core and shell sizes can result in the same emission wavelength. The ability to resolve these peaks in ensemble PLE spectra gives further evidence that the synthesis of nearly monodisperse cores combined with the SILAR shells result in extremely high quality colloidal heterostructures.

The difference between absorption and PLE spectra, given the low size distribution of the QDs used in this study suggests that alternative explanations are necessary. In previous work, scattering from aggregates of type-I CdSe QDs and ligands was hypothesized to be responsible for differences between the PLE spectra and the absorption spectra in CdSe QDs at room temperature [30]. In this study, the effect of scattering on the discrepancy between PLE and absorption spectra of CdTe/CdSe QDs was found to be minimal. After successive purifications using precipitation and redissolution, no change in either the absorption or PLE spectra was noticed, in contrast to findings for CdSe QDs.

3.5. Lifetime measurements

Lifetime measurements allow us to probe the degree of wavefunction overlap of the carriers, or the oscillator strength of the transition. According to Efros, the wavefunction overlap integral is directly proportional to the radiative lifetime in QDs [31,32]. With increasing type-II nature, it is expected that the wavefunction overlap between the electron and hole decreases because of larger charge separation, giving longer lifetime values. Ultrafast nonradiative processes should also be significantly reduced in CdTe/CdSe in which there is large spatial separation between electrons and holes, since Auger nonradiative decay is strongly dependent on Coulomb interactions. According to Kim et al. [24], hole-trap mediated nonradiative decay processes should be suppressed for CdTe/CdSe QDs since holes are confined away from the surface.

In previous work on CdTe/CdSe QDs, lifetime data were fit with a stretched exponential function, showing only one component to the fluorescence lifetime [24]. In this study, multiple exponent lifetimes could be extracted (Table 1), as previously found for type-I CdSe NCs [33]. Nearly identical trends of changes in the longest lifetime component (as seen in Table 1 and Fig. 6(b)) could be found for three sets of sample batches. However, fitting with a stretched exponential function did not lead to acceptable fits for all data presented for SILAR-grown CdTe/CdSe QDs as shown by the residuals (Acceptable fits are shown in Table 2, residuals are compared in supporting information). Meanwhile, multi-exponential fitting led to acceptable fits for all samples studied. It was found that the minimal but sufficient number of exponents needed for an acceptable fit was four: $f(t) = \sum_{i=1}^{4} A_i e^{-(t/\tau_i)}$.

Recombination of carriers from the core/shell interface is expected to result in the longest lifetime component, and shorter lifetime components in type-II structures may be attributed to fast surface/interface trapping processes as suggested by Balet et al. [32]. The redshift of the photoluminescence peaks as a function of shell thickness (Fig. 4) indicates reduction in quantum confinement due to larger size, i.e., lowering of the CdSe conduction band minimum with respect to CdTe conduction band minimum. This should create a larger barrier for the electrons to tunnel through and recombine with holes in the CdTe core. Because of this increasing barrier height, it is expected that the wavefunction overlap between the electron and the hole should be very sensitive to small changes in shell thickness. It was previously found for CdSe/ZnTe type-II QDs, that changing the core diameter while keeping the shell thickness constant had no appreciable effect on the fluorescence lifetimes [34]. Meanwhile, increasing the core diameter without the ZnTe shell resulted in shorter lifetimes. Increasing the core size of these structures lowers the energy of the conduction band and redshifts their emissions. Given the above arguments, the lifetime results for CdSe/ZnTe seem surprising.

In contrast, we observe for CdTe/CdSe QDs longer lifetimes for longer wavelength emissions. These results suggest an increase in the conduction band offset between the two layers as shell thickness is increased (Table 1). CdTe cores have shorter lifetimes (with longest components $\tau_3 = 9$ ns and $\tau_4 = 33$ ns) than found for type-II structures. It was found that each additional monolayer of CdSe overcoating CdTe cores significantly increases the longest (τ_4) lifetime component (Fig. 6 and Table 1) of these QDs. τ_4 increases from 33 to 87 ns going from 0 monolayers to 4 monolayers of CdSe. A striking result found in this study is that even adding half a monolayer shell (from 2.5 to 3) changes the lifetimes drastically (τ_4 increases from 54 to 71 ns). We expected that adding an extra, higher band gap type-I shell on top of type-II structures may effectively confine electrons in the quantum dot, thereby causing changes in the lifetimes. However, the core/shell/shell CdTe/CdSe/CdS structure exhibited longer lifetimes than CdTe/CdSe with the same number of CdSe shell monolayers (Table 1). The longer lifetimes and the additional photoluminescence redshift with the addition of second CdS shell suggest electron wavefunction leakage through that shell. Since there is less oscillator strength measured by the extended lifetimes, one would expect the QYs to

Table 1
Values extracted from four exponent fits to lifetime data of CdTe cores, CdTe/CdSe with 1–4 monolayers of CdSe shells, and CdTe/CdSe/CdS QDs with 1–2 monolayers of CdS shells

Sample	Emission peak (nm)	A_1 (%)	τ_1 (ns)	A_2 (%)	τ_2 (ns)	A_3 (%)	τ_3 (ns)	A_4 (%)	τ_4 (ns)
CdTe	687	20.9	0.00	51.5	1.15	17.2	8.72	10.4	**32.76**
CdTe/CdSe (1)	700	22.7	0.00	41.4	1.67	17.4	13.77	18.4	**40.66**
CdTe/CdSe (2)	722	58.3	0.00	10.8	2.59	13.6	25.11	17.4	**52.79**
CdTe/CdSe (2.5)	735	48.0	0.00	5.4	11.91	36.1	34.34	10.4	**53.60**
CdTe/CdSe (3)	755	65.9	0.00	8.0	2.81	9.7	28.37	16.5	**70.64**
CdTe/CdSe (4)	802	40.0	0.00	30.0	2.10	13.3	22.60	17.2	**86.63**
CdTe/CdSe/CdS (4/1)	819	78.2	0.00	7.9	2.96	6.6	25.03	7.2	**99.09**
CdTe/CdSe/CdS (4/2)	822	51.3	0.00	19.2	3.57	14.6	27.20	14.8	**99.64**

Values for the longest lifetime component (τ_4), reflecting changes due to shell thickness, are shown in bold font.

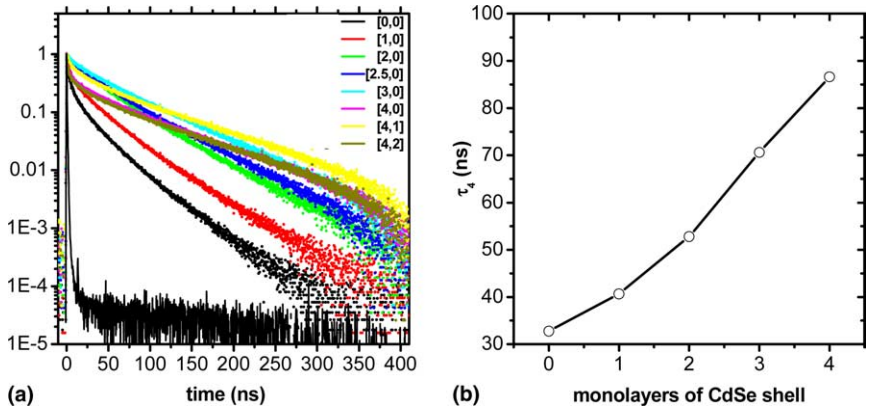

Fig. 6. (a) Lifetime data on CdTe cores, CdTe/CdSe with 1–4 monolayers of CdSe, and CdTe/CdSe/CdS QDs The instrument response function (solid line) is plotted with the lifetimes of the quantum dots. In the notation $[x, y]$, x is the layers of CdSe and y is the layers of CdS. (b) Plot of the longest lifetime component (τ_4) vs. number of monolayers of CdSe shell deposited on CdTe cores.

Table 2
Values extracted from stretched exponent fits ($f(t) = Ae^{-(t/\tau)^{(1-\beta)}}$) to lifetime data of selected samples

Sample	τ (ns)	Beta
CdTe/CdSe (2)	31.93	0.81
CdTe/CdSe (2.5)	35.03	0.79
CdTe/CdSe (3)	44.08	0.79
CdTe/CdSe/CdS (4/1)	30.62	0.55

be lower than those of the cores for a purely radiative process. However, the slightly higher QYs and increased photostability suggest that the CdS shell effectively passivates surface defects and reduces nonradiative decay processes.

4. Conclusion

The layer by layer synthesis of type-II CdTe/CdSe QDs using the SILAR technique enables us to study wavefunction engineering in the quantum size regime. Photoluminescence excitation spectra can resolve excitonic states in type-II structures that are hidden in the absorption spectra. Systematic changes of lifetime with shell growth of the type-II layer demonstrates high level excitonic wavefunction manipulation and radiative recombination control. The degree of bandgap and wavefunction engineering demonstrated here could prove useful in the development of near-infrared fluorescent probes of different colors and different lifetimes, possessing ideal properties for in vitro and in vivo biological and medical applications.

Acknowledgements

This work was supported with funding from the National Institute of Health, Grant No. 5-R01 EB000312-04, DARPA and AFOSR, Grant No. FA955004-10048. We also acknowledge the W.M. Keck Foundation for their support to this work from the W.M. Keck Epithelial Cell Cancer Biology Program at UCLA (Grant # 04074070). The authors thank Dr. Guido Zampighi and Dr. Sirus Kohan for providing accesses to their TEM facilities.

Appendix A. Supplementary data

Supplementary data associated with this article can be found, in the online version, at doi:10.1016/j.chemphys.2005.04.029.

References

[1] Z.I. Alferov, Semiconductors 32 (1998) 1.
[2] A.Y. Cho, Journal of Vacuum Science and Technology 8 (1971) 31.
[3] A.Y. Cho, Applied Physics Letters 19 (1971) 467.
[4] H.M. Manasevit, Applied Physics Letters 12 (1968) 156.
[5] D.S. Chemla, A. Maruani, Progress in Quantum Electronics 8 (1982) 1.
[6] D.S. Chemla, Journal of Luminescence 30 (1985) 502.
[7] D.S. Chemla, Physics Today 46 (1993) 22.
[8] D.A.B. Miller, D.S. Chemla, T.C. Damen, A.C. Gossard, W. Wiegmann, T.H. Wood, C.A. Burrus, Physical Review Letters 53 (1984) 2173.
[9] D.A.B. Miller, D.S. Chemla, T.C. Damen, A.C. Gossard, W. Wiegmann, T.H. Wood, C.A. Burrus, Applied Physics Letters 45 (1984) 13.
[10] W.H. Knox, C. Hirlimann, D.A.B. Miller, J. Shah, D.S. Chemla, C.V. Shank, Journal of the Optical Society of America B-Optical Physics 3 (1986) P42.
[11] D.S. Chemla, J. Shah, Proceedings of the National Academy of Sciences of the United States of America 97 (2000) 2437.
[12] D.S. Chemla, J. Shah, Nature 411 (2001) 549.
[13] L.V. Butov, C.W. Lai, A.L. Ivanov, A.C. Gossard, D.S. Chemla, Nature 417 (2002) 47.
[14] L.V. Butov, A.C. Gossard, D.S. Chemla, Nature 418 (2002) 751.

[15] R.A. Kaindl, M.A. Carnahan, D. Hagele, R. Lovenich, D.S. Chemla, Nature 423 (2003) 734.
[16] C.W. Lai, J. Zoch, A.C. Gossard, D.S. Chemla, Science 303 (2004) 503.
[17] B.A. Wilson, IEEE Journal of Quantum Electronics 24 (1988) 1763.
[18] D.A.B. Miller, D.S. Chemla, S. Schmittrink, Journal of the Optical Society of America B-Optical Physics 3 (1986) P42.
[19] D.A.B. Miller, D.S. Chemla, S. Schmittrink, Applied Physics Letters 52 (1988) 2154.
[20] A.P. Alivisatos, Science 271 (1996) 933.
[21] M. Bruchez, M. Moronne, P. Gin, S. Weiss, A.P. Alivisatos, Science 281 (1998) 2013.
[22] W.C.W. Chan, S.M. Nie, Science 281 (1998) 2016.
[23] X. Michalet, F. Pinaud, L.A. Bentolila, J.M. Tsay, J.J. Li, S. Doose, S. Weiss, Science 307 (2005) 538.
[24] S. Kim, B. Fisher, H.-J. Eisler, M. Bawendi, Journal of the American Chemical Society 125 (2003) 11466.
[25] S. Kim, Y.T. Lim, E.G. Soltesz, A.M. De Grand, J. Lee, A. Nakayama, J.A. Parker, T. Mihaljevic, R.G. Laurence, D.M. Dor, L.H. Cohn, M.G. Bawendi, J.V. Frangioni, Nature Biotechnology 22 (2004) 93.
[26] J.J. Li, Y.A. Wang, W.Z. Guo, J.C. Keay, T.D. Mishima, M.B. Johnson, X.G. Peng, Journal of the American Chemical Society 125 (2003) 12567.
[27] D. Battaglia, J.J. Li, Y.J. Wang, X.G. Peng, Angewandte Chemie-International Edition 42 (2003) 5035.
[28] W.W. Yu, Y.A. Wang, X.G. Peng, Chemistry of Materials 15 (2003) 4300.
[29] D.J. Milliron, S.M. Hughes, Y. Cui, L. Manna, J.B. Li, L.W. Wang, A.P. Alivisatos, Nature 430 (2004) 190.
[30] D. Tonti, F. van Mourik, M. Chergui, Nano Letters 4 (2004) 2483.
[31] A.L. Efros, Physical Review B 46 (1992) 7448.
[32] L.P. Balet, S.A. Ivanov, A. Piryatinski, M. Achermann, V.I. Klimov, Nano Letters 4 (2004) 1485.
[33] M.A. Hines, P. Guyot-Sionnest, Journal of Physical Chemistry 100 (1996) 468.
[34] C.Y. Chen, C.T. Cheng, J.K. Yu, S.C. Pu, Y.M. Cheng, P.T. Chou, Y.H. Chou, H.T. Chiu, Journal of Physical Chemistry B 108 (2004) 10687.